Cavitation Dynamics at Microscale Level

Georges L. Chahine

Dynaflow, Inc., Fulton, Maryland and John Hopkins University, Baltimore

Cavitation in a liquid is known for its deleterious effects, namely erosion, noise and loss of performance. In a mechanical heart valve, stresses generated by cavitation could lead to catastrophic failure. These deleterious effects are directly connected to the dynamics of pre-existing microscopic nuclei in the liquid medium. To highlight this, a selective review of the dynamics of the bubbles at the microscopic levels is considered here; the various aspects of the problem are highlighted and briefly addressed; new areas of research in non-spherical and bubble cloud dynamics are then considered. The importance of the inclusion of these collective and non-uniform flow effects in the dynamics of bubbles in a realistic cavitating flow field is also elucidated.

The Journal of Heart Valve Disease 1994;3 (Suppl. I): S 102-116

Cavitation and bubble dynamics have been the subject of extensive research since the early works of Besant (1) and Lord Rayleigh (2). The phenomenon has been studied mostly for hydrodynamic applications, where its presence is associated with deleterious effects; i.e. performance deterioration, material erosion, and noise generation. More recently, cavitation has been studied for useful purposes including sound generation, cutting, drilling, cleaning, enhancement of mixing and chemical reactions, emulsification, etc. (3-8).

This article studies the damaging effects of cavitation on implants such as mechanical heart valves, and its negative effects on biological cells and tissue in vivo. In both these cases stresses generated by cavitation lead to undesirable effects; in a mechanical heart valve, failure of the valve could result from the development of cracks, while cells could be damaged or induced to collect around bubbles.

This presentation does not intend to be a complete and inclusive review of the phenomenon of cavitation. Instead it will consider some aspects of the subject relevant to cavitation erosion from a microscopic point of view of the bubble dynamics. Our aim is to give an overview of the problem areas where significant knowledge has been accumulated and to discuss important aspects of the dynamics which either have not yet been addressed properly or are the subject of on-going intensive research.

Address for correspondence:
Georges L. Chahine, Dynaflow Inc., 7210 Pindell School Road, Fulton, Maryland 20759, USA

Cavitation inception

Background

Despite a large number of investigations and publications on the subject - including several well documented books and review articles (6-9) - the fundamentals of cavitation remain relatively poorly understood. In order to achieve a cavitation-free design of a submerged body (such as a valve, propeller, etc.), or to simulate cavitation and test a model scale in a laboratory environment, it is necessary to establish criteria for cavitation inception, and to define scaling parameters between model and full scale. From talking to engineers and practitioners of fields where cavitation is a problem, the most commonly used definition of cavitation is based on an over-simplification that serves the purpose in most engineering cases but could lead to erroneous conclusions if used to explain or model new problems areas. This traditional engineering definition is that a liquid flow experiences cavitation if the local pressure drops below the liquid vapor pressure, p_v.

Definition of the cavitation number

A dimensional analysis of the flow around an obstacle (e.g. foil or a valve) of streamwise and transverse characteristic length scales, L and W, shows that the pressure, p_M, at any point M, can be written as a function, $\mathcal{F}$, of the following variables:

$$p_M = \mathcal{F}\,(P_\infty,\alpha,L,W,\rho,V_\infty,\mu), \qquad (1)$$

where α is the incidence angle of the flow relative to the obstacle, P_∞ and V_∞ are the characteristic pressure and

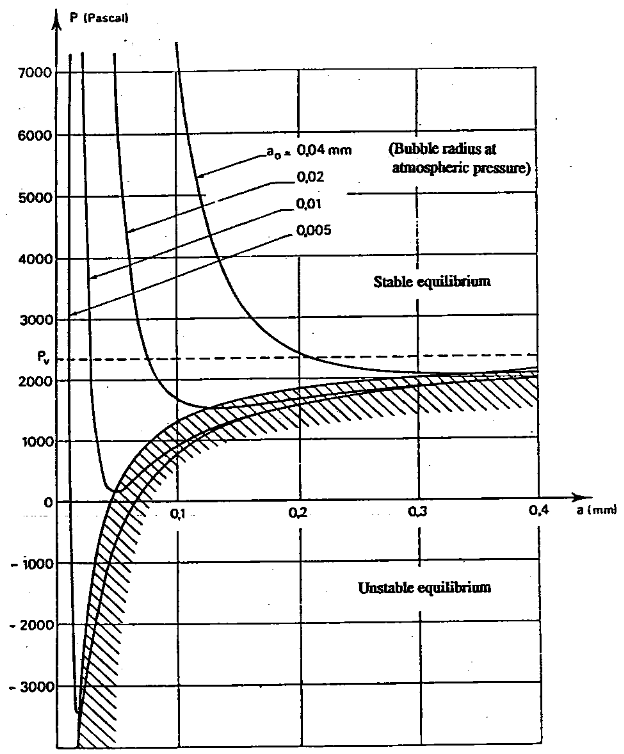

Figure 1: Curves of bubble static equilibrium.

velocity of the flow, respectively, and ρ and μ are the liquid density and kinematic viscosity, respectively. Based on the above engineering definition of cavitation, from a cavitation inception standpoint, any pressure, p_M, in the liquid flow is important only in terms of the pressure difference, p_M - p_v, since the liquid cavitates when $p_M = p_v$. In this case, Equation (1) becomes at the inception of cavitation:

$$\frac{P_\infty - P_v}{\frac{1}{2}\rho V_\infty^2} = \mathcal{F}\left(\alpha, \frac{W}{L}, \frac{\rho V_\infty L}{\mu}\right), \quad \text{or} \quad \sigma = \mathcal{F}(\alpha, \mathcal{G}, \mathcal{R}_e). \quad (2)$$

$\mathcal{R}_e$ is the Reynolds number, $\mathcal{G}$ is a geometric characteristic (shape parameter) of the obstacle, and σ is the "cavitation number" defined as:

$$\sigma = \frac{p_\infty - p_v}{\frac{1}{2}\rho V_\infty^2} \quad (3)$$

Scaling various cavitation experiments or a model configuration to a full scale configuration is obtained by conserving σ.

Presence of cavitation nuclei

The above definition of cavitation inception is only true in static conditions when the liquid is in contact with its vapor through the presence of a large free surface. For the more common condition of a liquid in a flow, or in a biological application, liquid vaporization can only occur through the presence of "micro free surfaces" or microbubbles, also called "cavitation nuclei". Indeed, a pure liquid free of nuclei can sustain very large tensions, measured in hundreds of atmospheres, before a cavity can be generated through separation of the liquid molecules. Therefore, any fundamental analysis of cavitation inception has to start from the observation that any real liquid contains nuclei which when subjected to variations in the local ambient pressure will respond dynamically by oscillating and eventually growing explosively (i.e. cavitate). A more precise definition is presented in the next section.

Cavitation inception appears under several forms, the most recognized being (14):

(a) Explosive growth of individual bubbles,
(b) Sudden appearance of transient cavities or "flashes" on boundaries,
(c) Sudden appearance of attached partial cavities, or sheet cavities,
(d) Explosive growth of bubble clouds, behind attached cavities or a vibrating surface.
(e) Sudden appearance of rotating filaments, or vortex cavitation.

Upon further analysis, all these forms can be related to the explosive growth of pre-existing nuclei in the liquid when subjected to pressure drops generated by various forms of local pressure disturbances. These are either acoustically imposed pressure variations (ultrasound applications), uniform pressure drops due to local liquid accelerations, or strongly non-uniform pressure fields due to streamwise or transverse large vortical structures. The presence of nuclei or weak spots in the liquid is therefore essential for cavitation inception to occur when the local pressure in the liquid drops below some critical value, p_c, which is addressed next.

Bubble static equilibrium

The first level of sophistication for the definition of a cavitation inception criterion is based on the concept of static equilibrium of a bubble in a liquid. The criterion predominantly used is based on a spherical bubble model, even though it applies only to a limited number of the cavitation forms listed above. In this model, the bubble is assumed to contain non condensable gas of partial pressure, P_g, and vapor of the liquid of partial pressure, p_v (6-9). Therefore, at any point M on the bubble surface, the balance between the internal pressure, the liquid pressure, and surface tension can be written:

$$P_{L_0} = p_v + P_{g_0} - \frac{2\gamma}{R_0}, \quad (4)$$

where P_{L_0} is the pressure in the liquid, γ is the surface tension parameter, and R_0 is the bubble radius.

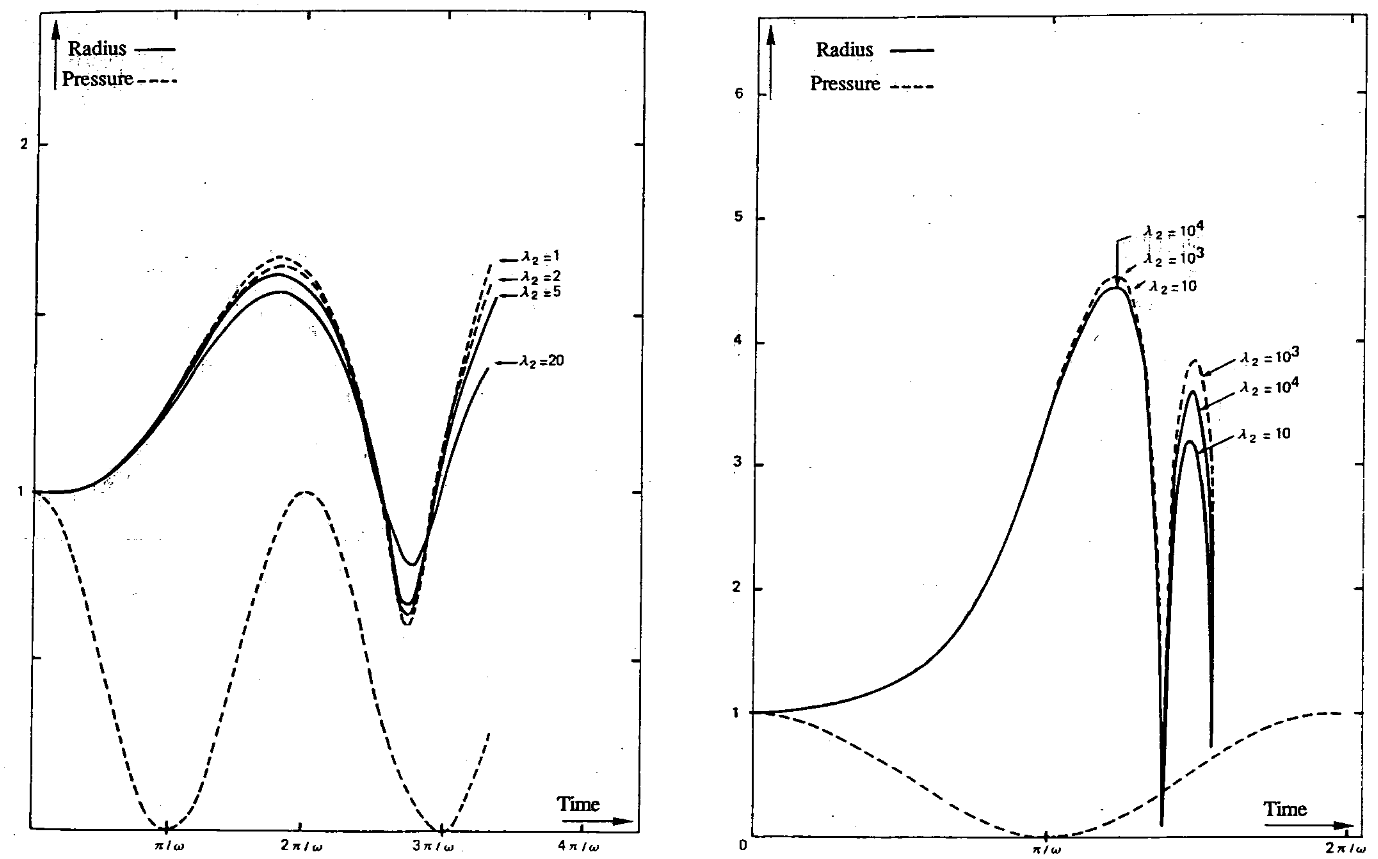

Figure 2: Influence of viscoelastic properties on spherical bubble dynamics. λ_1 and λ_2 *correspond to Newtonian fluid. a) Bubble oscillations case;* $\lambda_1 = 2$. *b) Bubble collapse case;* $\lambda_1 = 10^3$. *Reprinted from (10).*

If the liquid ambient pressure changes very slowly, the bubble radius will change accordingly to adapt to the new value. This is accompanied by a modification of the pressure inside the bubble. The vaporization of the liquid at the bubble-liquid interface occurs very fast relative to the time scale of the bubble dynamics, so that the liquid and the vapor can be considered in equilibrium at every instant, and the partial pressure of the vapor in the bubble is always constant. On the other hand, gas diffusion occurs over a much longer time scale, so that the amount of gas inside the bubble remains constant. This results in a gas partial pressure which varies with the bubble volume. Since we are interested in a quasi-steady equilibrium, P_g is considered to follow an isothermal compression law, and is related to the reference value, P_{go}, and to the new bubble radius R, through:

$$P_g = Pg_o\left(\frac{R_o}{R}\right)^3. \tag{5}$$

The dynamic equation at the bubble wall becomes:

$$P_L(R) = P_v + P_{g_o}\left(\frac{R_o}{R}\right)^3 - \frac{2\gamma}{R}, \tag{6}$$

where the notation, P_L(R), is meant to associate the liquid pressure, P_L, to the bubble radius, R.

An understanding of the bubble stable equilibrium can be obtained by considering the curve, $P_L(R)$. As illustrated in Figure 1, this curve has a minimum below which there is no equilibrium bubble radius. Only the left side branch of the curve corresponds to a stable equilibrium.

If the pressure in the flow field drops below the minimum of the curve, or critical pressure, p_c, an explosive bubble growth (cavitation) is provoked. This provides an improved definition for cavitation inception which depends on the size of the nuclei. The "critical pressure" is obtained by solving for the minimum of P_L(R), using Equation (6) and can be expressed as:

$$p_c = p_v - \frac{4\gamma}{3r_c}, \tag{7}$$

where γ is the surface tension parameter, and r_c is the "critical radius" given by:

$$r_c = \left[\frac{3R_o^3}{2\gamma}\left(P_{L_o} - p_v + \frac{2\gamma}{R_o}\right)\right]^{1/2}. \tag{8}$$

For a given ambient pressure, P_{Lo}, any bubble larger

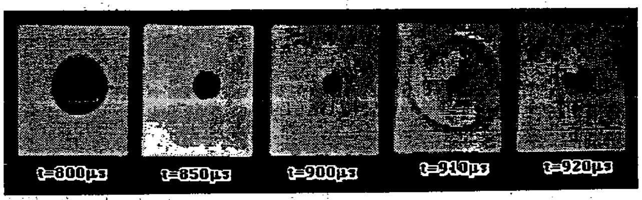

Figure 3: Emission of a shock wave during bubble collapse and rebound. Reprinted from (13).

than r_c will cavitate. This definition is much more accurate than the engineering definition, but lacks consideration of any dynamic or non-spherical effects, which can be predominant in some situations.

This new definition of cavitation inception highlights the fact that a correct scaling of the cavitation phenomenon has to account not only for the conservation of the parameters shown in Equation (2), but also for the nuclei size distribution between the model and the full scale.

Spherical bubble dynamics

Newtonian incompressible model - Rayleigh-Plesset equation

The most commonly used bubble dynamics model is based on the assumption of a spherical bubble in an incompressible liquid. In this case, the radial velocity of the liquid, u_r, at a distance, r, from the bubble center, is directly related to the bubble wall velocity through the continuity, or mass conservation equation:

$$ur = \dot{R}(t)\left[\frac{R(t)}{r}\right]^2, \tag{9}$$

where $R(t)$ is the bubble radius at time t, and $\dot{R}(t)$ is the bubble wall velocity. This equation accounts for the kinematic condition at the bubble wall - i.e. the velocity of the bubble wall is identical to the liquid velocity at this wall. This obviously neglects any flow (mass transfer) across the bubble interface. A second boundary condition at the bubble wall, which is dynamic, expresses the balance of the normal stresses at the wall. For a Newtonian fluid it can be written:

$$P_L(R) + 4\mu\frac{\dot{R}}{R} = P_i - \frac{2\gamma}{R}, \tag{10}$$

where P_L(R) is the pressure in the liquid at the bubble wall, P_i the pressure inside the bubble, γ the surface tension, and μ the kinematic viscosity. As above, the bubble contains vapor of the liquid at the constant partial pressure, p_v, and non-condensable gas at the partial pressure, P_g, which is related to the reference value P_{go} through:

$$P_g = P_{go}\left(\frac{\mathcal{V}_o}{\mathcal{V}}\right)^k, \tag{11}$$

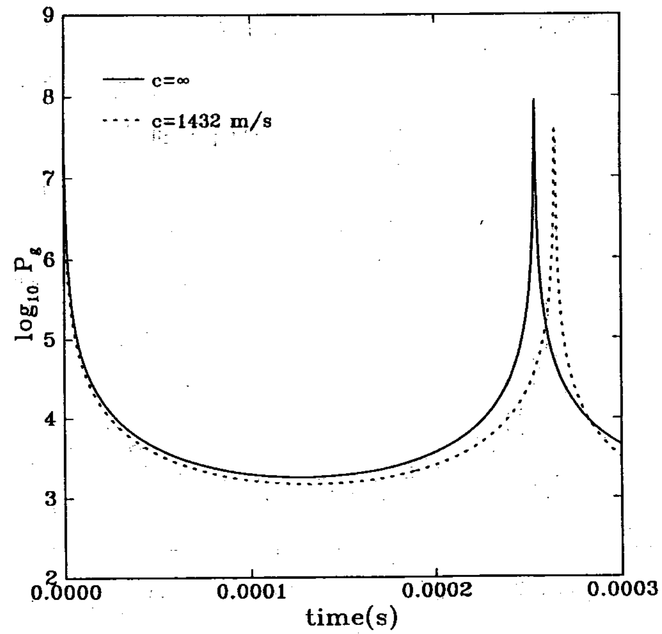

Figure 4: Gas pressure inside the bubble as a function of time for a bubble subjected to a sudden pressure drop. Comparison between an incompressible medium case (c=[infinity]) and a compressible medium.

where the constant k is between 1.0 (isothermal) and c_p/c_v (adiabatic), and V_0 and V are the reference and instantaneous values of the bubble volume respectively.

The pressure balance at the bubble interface then becomes:

$$P_L(M) = P_v + P_{go}\left(\frac{R_o}{R}\right)^{3k} - \frac{2\gamma}{R} - 4\mu\frac{\dot{R}}{R}. \tag{12}$$

A number of effects such as gas diffusion or heat transfer have been neglected in the above equation, and are usually unimportant in the case of a growing and collapsing bubble in a cold liquid. For an oscillating bubble, however, rectified diffusion can be very important.

If we replace Equation (9) in the liquid momentum equation, integrate that equation between the radius of the bubble and infinity where the imposed pressure is P_∞(t), and account for Equation (11), we obtain the well known Rayleigh-Plesset (RP) Equation (2,9) where dots denote time derivatives:

$$\rho\left[R\ddot{R} + \frac{3}{2}\dot{R}^2\right] + 4\mu\frac{\dot{R}}{R} = P_{go}\left(\frac{R_o}{R}\right)^{3k} + P_v - P_\infty(t) - \frac{2\gamma}{R}. \tag{13}$$

This differential equation describes the bubble radius versus time when the time variations of P_∞ are known. Integration of this equation enables one to obtain conditions for bubble oscillations, or rapid bubble growth and collapse. In addition, this equation provides the necessary input to compute the pressure generated

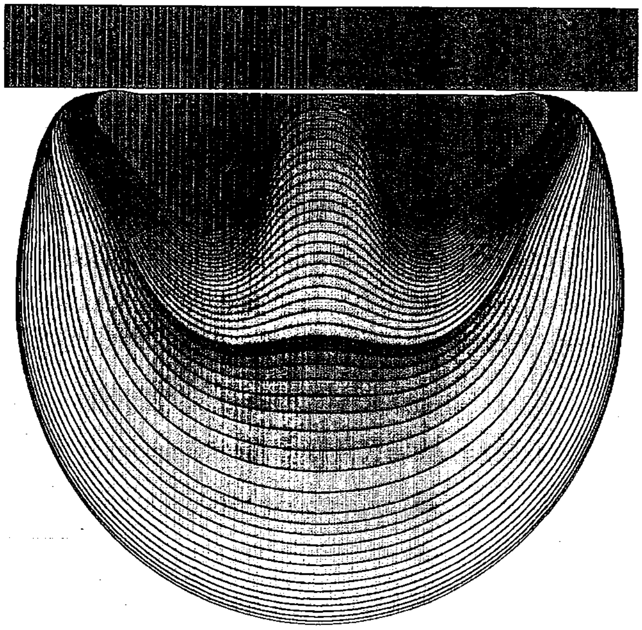

Figure 5: Numerical simulation of bubble collapse near a solid wall using 2DynaFS. Bubble contours at various times during collapse.

during bubble collapse. These pressures can be very large. They decrease with an increase in the amount of initial gas in the bubble. They will be considered as reference values in comparison with other models in the following sections.

Viscoelastic liquid: modified RP equation

When the liquid in which cavitation occurs does not have Newtonian properties, the above RP dynamics equation must be modified to account for a non-linear stress-strain relationship. This is the case for instance in blood flow, or in hydrodynamics when polymer additives are used to reduce drag. The question is then to evaluate to what extent accounting for the fluid's non-Newtonian behavior is important from the cavitation view point. In previous studies (10-12), we considered theoretically (10), and experimentally the behavior of spherical and non-spherical (11,12) bubbles in a viscoelastic fluid medium. The equation of state of the fluid was taken to be a general 3-parameter Oldroyd model such that the stress-strain relationship (σ and e are the stress and strain tensors) is given by:

$$\sigma_{ij}^{D} + \tau_g \frac{d\sigma_{ij}^{D}}{dt} = 2\mu \left(e_{ij}^{D} + \theta_g \frac{de_{ij}^{D}}{dt} \right) \qquad (14)$$

where τ_g, $\tau\eta_g$, and μ are characteristic relaxation times and the dynamic viscosity of the non-Newtonian fluid. For a spherical bubble this fluid behavior shows up in both the momentum equation:

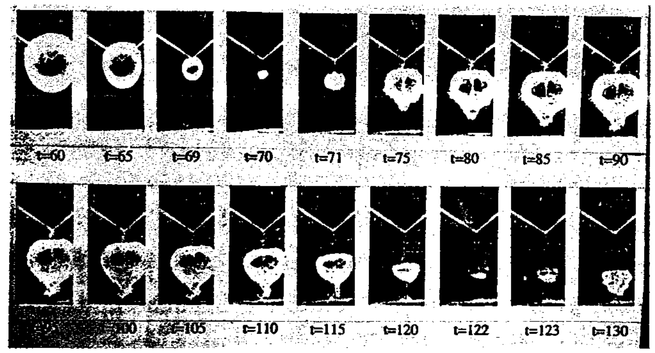

Figure 6: High speed photographs of bubble collapse near a solid wall using a spark-generated bubble.

$$\rho \left[\frac{\partial u}{\partial t} + u \frac{\partial u}{\partial r} \right] = -\frac{\partial p}{\partial r} + \frac{\partial \sigma_{rr}^{D}}{\partial r} + \frac{3\sigma_{rr}^{D}}{r}, \qquad (15)$$

where the last two terms have replaced the more conventional viscous terms, and in the stress balance equation at the bubble interface, which becomes:

$$P_L(M) = P_{go} \left(\frac{R_o}{R} \right)^{3k} + P_v - \frac{2\gamma}{R} - \sigma_{rr}^{D}. \qquad (16)$$

Finally, for an incompressible isolated bubble the differential equation describing the bubble radius versus time becomes:

$$\rho \left[R\ddot{R} + \frac{3}{2}\dot{R}^2 \right] = P_{go} \left(\frac{R_o}{R} \right)^{3k} + P_v - \frac{2\gamma}{R_o} - P_\infty(t)$$
$$- 4\mu \left[\frac{\theta_g}{\tau_g} \frac{\dot{R}}{R} - \frac{\theta_g - \tau_g}{\tau_g^2} \int_0^t e^{(\alpha - t)/\tau_g} \right.$$
$$\left. \times \frac{R^2(\alpha)\dot{R}(\alpha)}{R^3(\alpha) - R^3(t)} \log \frac{R^3(\alpha)}{R^3(t)} \, d\alpha \right]. \qquad (17)$$

Figure 2 shows a comparison between the oscillation and collapse of a spherical bubble in a viscoelastic liquid and water. Negligible effects are seen for a strong bubble collapse unless for very large unrealistic values of $\lambda_1 = \tau_g\rho\sigma^2/64\mu^3$ and $\lambda_2 = \tau\eta_g\rho\sigma^2/64\mu^3$. Viscoelastic effects appear less negligible for weaker bubble oscillations, and when several bubble periods are considered (10). Experimental results relative to the viscoelastic effects are presented below.

Influence of liquid compressibility

Even though generally neglected in bubble dynamics studies, compressibility of the liquid medium can become important when the speed of the bubble wall during collapse or rebound approaches the sound speed in the liquid. This is illustrated in Figure 3, where shock waves are emitted at bubble collapse (13). In order to model the liquid compressibility, an equation

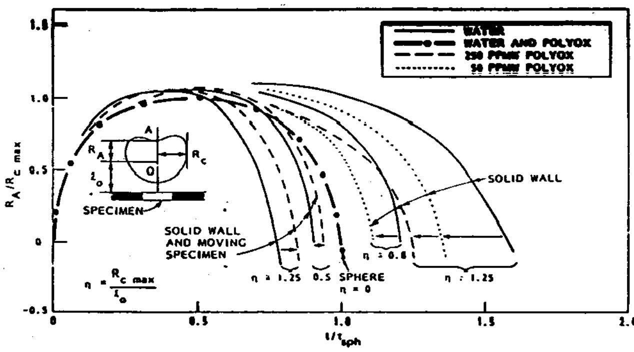

Figure 7: Motion of the re-entering jet point in the presence of a moving and rigid solid wall. Influence of the addition of a polymer solution. Reprinted from (12).

of state of the liquid is introduced. For instance, for water the following Tait equation (6-8) is used:

$$\frac{p+B}{p_\infty + B} = \left(\frac{\rho}{\rho_\infty}\right)^n, \qquad (18)$$

in which B and n are constants depending upon the liquid, with values of 3000 atmospheres and 7.25, respectively, for water. The model that has been shown to be the most precise, was proposed by Gilmore (15), and is based on the Kirkwood-Bethe (16) hypothesis. This hypothesis states that the disturbance of any fluid property propagates along an outgoing characteristic of velocity of propagation of $u + c$, the sum of the local velocity of the fluid and the sound speed. In this case the equation of motion of the bubble wall can be written:

$$R\ddot{R}\left(1-\frac{\dot{R}}{c}\right)+\frac{3}{2}\dot{R}^2\left(1-\frac{\dot{R}}{3c}\right) = H\left(1+\frac{\dot{R}}{c}\right)+\frac{R}{c}\frac{dH}{dt}\left(1-\frac{\dot{R}}{c}\right) \qquad (19)$$

where c is the sound speed at the bubble wall. H is the difference between the enthalpy at the bubble wall and at infinity, and with an isentropic liquid compression assumption is defined as:

$$H(p) = \int_{p_\infty}^{p} dh = \int_{p_\infty}^{p} \frac{dp}{\rho}. \qquad (20)$$

The pressure in the liquid is then given by the following equation at a given location r:

$$p(r) = (p_\infty + B)\left[\left(\frac{y}{r}-\frac{u^2}{2}\right)\left(\frac{n-1}{n}\frac{\rho_\infty}{p_\infty + B}\right)+1\right]^{n/(n-1)} - B. \qquad (21)$$

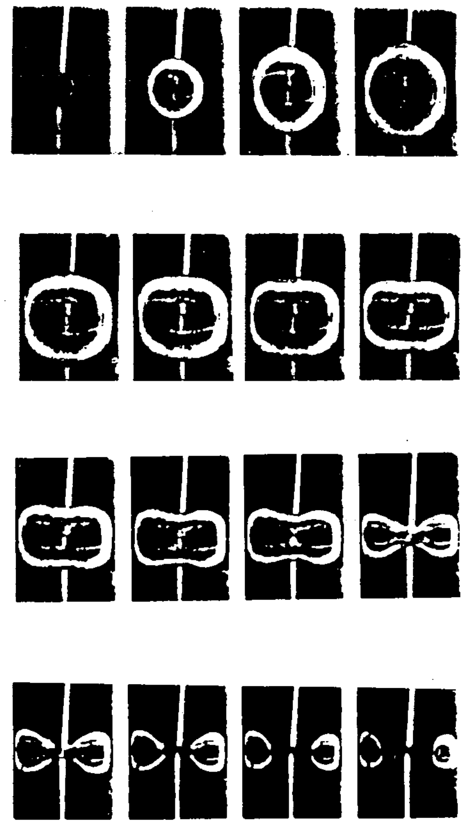

Figure 8: High speed photography observation of bubble dynamics between two solid walls.

The velocity of the fluid along the characteristic surface is given by:

$$\frac{du}{dt} = \frac{1}{c-u}\left[(c+u)\frac{y}{r^2} - 2\frac{c^2u}{r}\right], \qquad (22)$$

with $y = (h - u^2/2)/r$. Using as the initial condition the velocity and radius of the bubble wall, the above equation can be used to compute the velocity along the characteristic. Equation (20) then gives the corresponding pressures.

The former expressions reduce to the incompressible ones as the quantity $\dot{R}/c$ drops below 0.2. In general a slightly compressible model can be used to replace the Rayleigh-Plesset equation with the Keller-Herring equation (8):

$$\rho\left[\left(1-\frac{\dot{R}}{c}\right)R\ddot{R}+\frac{3}{2}\left(1-\frac{\dot{R}}{3c}\right)\dot{R}^2\right] = \frac{1}{\rho}\left(1+\frac{\dot{R}}{c}+\frac{R}{c}\frac{d}{dt}\right)[P_L - p_\infty], \qquad (23)$$

where:

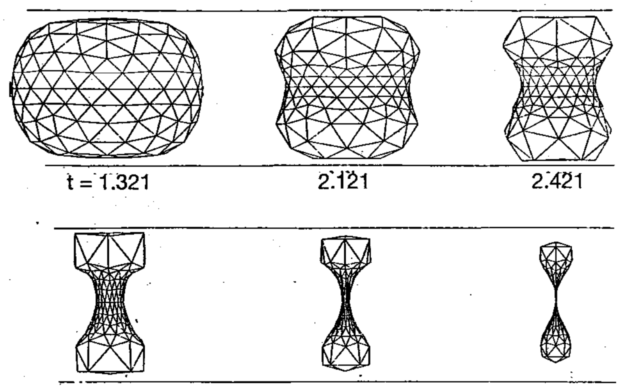

Figure 9: Numerical simulation using 3DynaFS of bubble dynamics between two solid walls.

$$P_L = P_{go}\left(\frac{R_0}{R}\right)^{3k} + P_v - \frac{2\sigma}{R}. \quad (24)$$

Figure 4 compares the pressures in the bubble when compressibility is taken into account and when it is not for a particular case of a spherical bubble collapse. Both an increase in the bubble period and a decrease in the maximum bubble pressure can be observed when a finite sound speed in the water is considered.

Non-spherical bubble dynamics

Introduction

In most practical applications where cavitation occurs, bubbles are seldom isolated or spherical. This is the case, for instance, in biological applications when blood flows in and out of the heart through a heart valve. During closure of the valve, flow separation and increased velocities can induce bubble nuclei explosive growth followed in the higher pressure regions by bubble collapse. Fortunately, with the recent advent of modern computational, experimental, and analytical techniques, the often-neglected bubble flow and bubble boundary interaction and deformation effects can be addressed. To do so, we developed a numerical method which accounts for strong bubble/bubble and bubble/flow interactions. This method has been used to date to study interaction between bubbles, bubbles and nearby rigid or deformable/movable boundaries, and bubble behavior in non-uniform flows when the underlying flow is viscous. Two particular shear flow cases of relevance to cavitation in separated flows are briefly considered here; a boundary layer flow near a flat wall and the flow field of a line vortex.

Shear and boundary interactions are probably important for flow around heart valves. In both cases significant modifications of the bubble dynamics are associated with the presence of the shear and its combined effects with nearby boundaries.

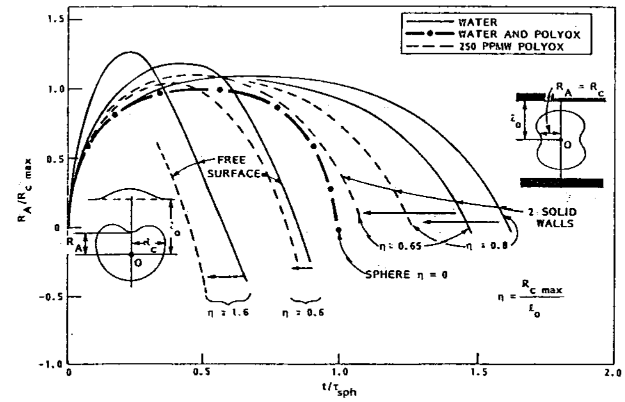

Figure 10: Motion of the re-entering jet point in the presence of two solid walls or free surface. Influence of the addition of a polymer solution. Reprinted from (12).

Bubble dynamics model: numerical boundary element method

For cavitation bubbles, large but subsonic bubble wall velocities are involved and, as a result, viscous and compressible effects in the liquid can be neglected. This results in a flow due to bubble dynamics that is potential (velocity potential, ϕ_b), and which satisfies the Laplace equation:

$$\nabla^2\phi_b = 0 \quad (25)$$

Boundary conditions are such that at all moving or fixed surfaces in the flow field an identity between fluid velocities normal to the boundary and the normal velocity of the boundary itself is to be satisfied. The bubble is assumed to contain non-condensable gas as well as vapor of the surrounding liquid, as above.

The three-dimensional Boundary Element Method developed (**3DynaFS**, with an axisymmetric version **2DynaFS** (17-19)) uses Green's equation to determine a solution to the Laplace equation. If the velocity potential, ϕ_b, and its normal derivatives are known on the fluid boundaries (points M), and ϕ_b satisfies the Laplace equation, then ϕ_b can be determined at any point P in the fluid domain using:

$$\int\int_S \left[-\frac{\partial\phi_b}{\partial n}\frac{1}{|MP|} + \phi_b\frac{\partial}{\partial n}\left(\frac{1}{|MP|}\right)\right] dS = \alpha\pi\phi_b(P), \quad (26)$$

$a\pi = \Omega$ is the solid angle under which P sees the fluid. The advantage of this integral representation is that it effectively reduces by one the dimension of the problem. If P is selected to be on the boundary of the fluid domain, then a closed system of equations is obtained and used at each time step to solve for values of $\delta\phi_b/n$ (or ϕ_b), assuming that all values of ϕ_b (or $\delta\phi_b/n$) are known at the preceding time step.

To solve Equation (26) numerically, the initially

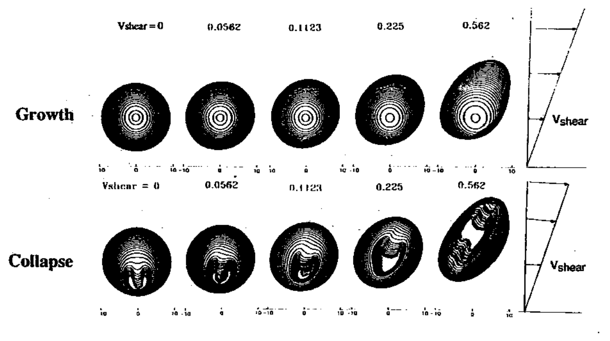

Figure 11: Influence of the presence of a linear shear velocity on the collapse of a bubble near a solid wall. V_{shear} is normalized with the Rayleigh velocity $\sqrt{\Delta P/\rho}$.

spherical bubble is discretized into a geodesic shape with flat, triangular panels. To evaluate the integrals in Equation (26) over any particular panel, linear variations of the potential and its normal derivative over the panel are assumed.

With the problem initialized and the velocity potential known over the surface of the bubble, an updated value of $\delta\phi_b/\delta n$ can be obtained by performing the integrations expressed above and solving the corresponding matrix equation. The unsteady Bernoulli equation can then be used to solve for $D\phi_b/Dt$, the total material derivative of δ_b while following a particular node during its motion. Using an appropriate time step, all values of ϕ_b on the bubble surface and all node positions can be updated. This time-stepping procedure is repeated throughout the bubble oscillation period, resulting in a shape history of the bubbles. The details of the numerics are described in a report by Chahine et al. (17).

Presence of a basic flow

To study bubble dynamics in a non-uniform flow field, the following model was used. Denoting the velocity of the non-uniform "basic flow" as V_o, and the resulting velocity field in the presence of oscillating bubbles as V_1, we defined the "bubble flow" velocity and pressure variables, V_b and P_b, as:

$$\mathbf{V}_b = \mathbf{V}_1 - \mathbf{V}_o, \qquad P_b = P_1 - P_0. \tag{27}$$

By noticing that, for cavitating flows, this "bubble flow" field can be considered to be a potential model, we were able to use a method similar to the one described in the previous section to study the dynamics. We then obtained the following modified Bernoulli equation (18,19,23):

$$\nabla\left[\frac{\delta\phi_b}{\delta t} + \frac{1}{2}|\mathbf{V}_b|^2 + \mathbf{V}_o \cdot \mathbf{V}_b + \frac{P_b}{\rho}\right] = \mathbf{V}_b \times (\nabla \times \mathbf{V}_o). \tag{28}$$

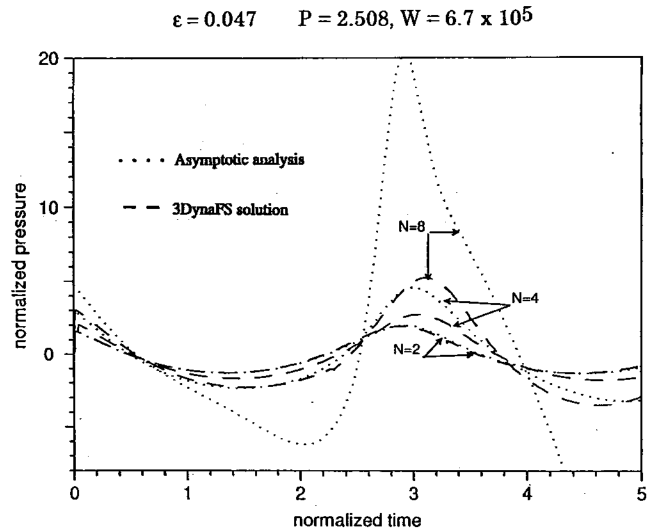

Figure 12: Comparison of the pressures at the cloud center predicted by 3DynaFS and the asymptotic analysis code. $\varepsilon = R_{max}/l_0 = 0.047$. Pressures are normalized by maximum value for isolated bubble. Reprinted from (24).

For cavitation in a line vortex, Equation (28) becomes (18):

$$\frac{\delta\phi_b}{\delta t} + \frac{1}{2}|\mathbf{V}_b|^2 + \frac{P_b}{\rho} = \text{constant along a radial direction.} \tag{29}$$

In the case of a flat wall boundary layer flow such that all velocity vectors are parallel to the wall (unit direction, e_x), and depend only on the distance, z, to the wall, $V_o = f(z).e_x$, Equation (28) becomes (19):

$$\frac{\partial\phi_b}{\delta t} + \frac{1}{2}|\mathbf{V}_b|^2 + \mathbf{V}_o \cdot \mathbf{V}_b + \frac{P_b}{\rho} = \text{constant along the } y \text{ direction.} \tag{30}$$

These two expressions were used in conjunction with the numerical model described above to conduct the simulations shown below.

Interaction with a nearby deformable structure

To study bubble interaction with deformable structures, the above described BEM codes were coupled to existing solid mechanics/structural dynamics codes, Nike3D and Nike2D, developed by Lawrence Livermore National Laboratories. These codes have the ability to include complex material and structure properties. The coupling between the two sets of codes is achieved through the dynamic condition at the boundaries of the deformable boundary. At these boundaries, the pressure from the liquid obtained through solution of the BEM liquid problem is used as the input or driving force for the structural model. The resulting

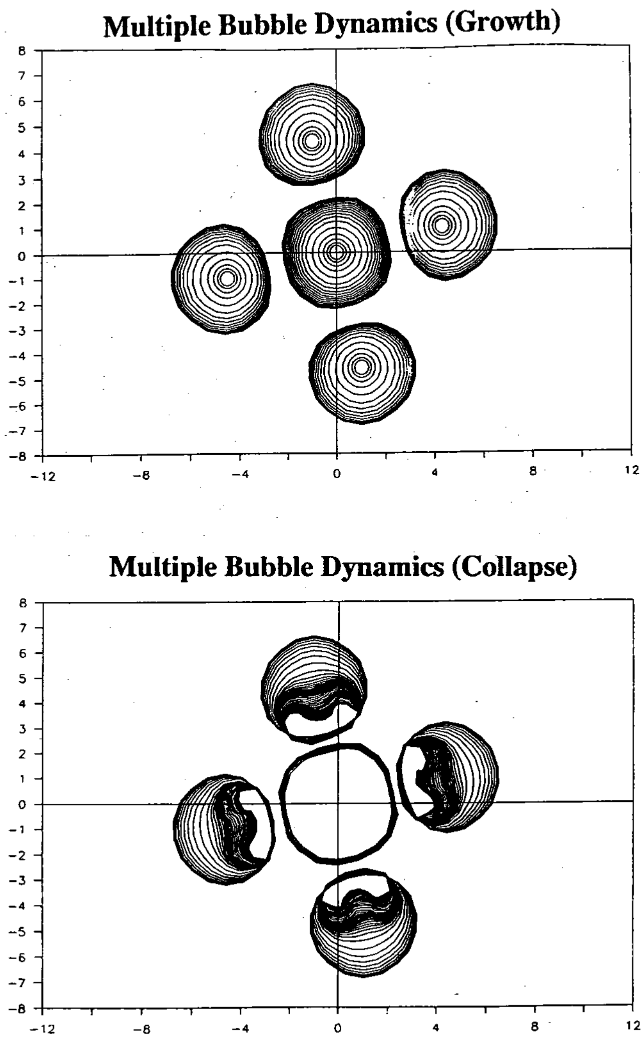

Figure 13: Growth and collapse of five bubbles having the same initial size and internal pressure. Influence of the initial bubble geometry distribution on dynamics. $\varepsilon = 0.474$, $P_{go}/P_{amb} = 283$. Reprinted from (23).

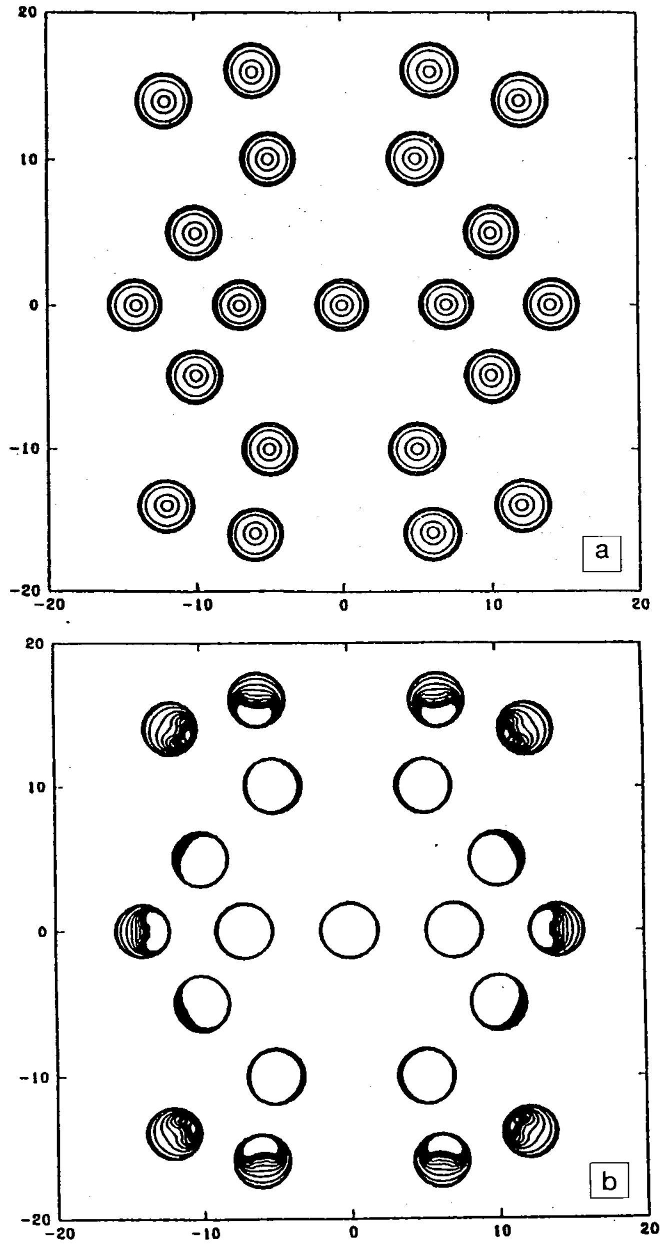

Figure 14: Simulation of the dynamic interactions between a cloud of 21 bubbles using 3DynaFS on a Cray. Two planes of symmetry are used; each bubble has 102 nodes and 200 panels. a) Growth. b) Collapse.

motion of the structure is then fed back into the BEM code to calculate the fluid motion at each time step, as described above. The velocity and position of each node are transferred to the fluid model. This coupling results in a fully interactive calculation (26).

Illustrative numerical results and experimental observations: spark-generated bubbles

In all the experiments reported here vapor bubbles (with some non-condensable gas) were generated in water by discharging a capacitor across a pair of platinum or tungsten electrodes for a very brief period of time. The generators used were capable of capacitor charge up to 10 kV. Such a system has been widely used by various authors for bubble dynamics studies, and the validity of the analogy between the collapse of the bubbles it produces and cavitation bubbles has been established (7). The electrodes were mounted in a large vessel which was hermetically sealed and connected to a vacuum pump. Lowering the ambient pressure was used for degasing and, when desired, for increasing the bubble size, thus slowing down the phenomena observed. This enabled the use of a moderate framing rate high-speed camera, a HYCAM, whose maximum capability was 10,000 frames per second.

Behavior near a solid wall

The physical mechanisms by which bubble collapse

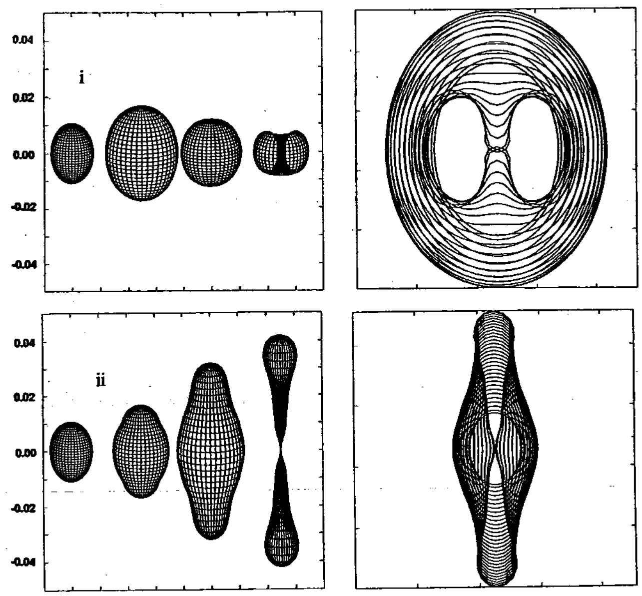

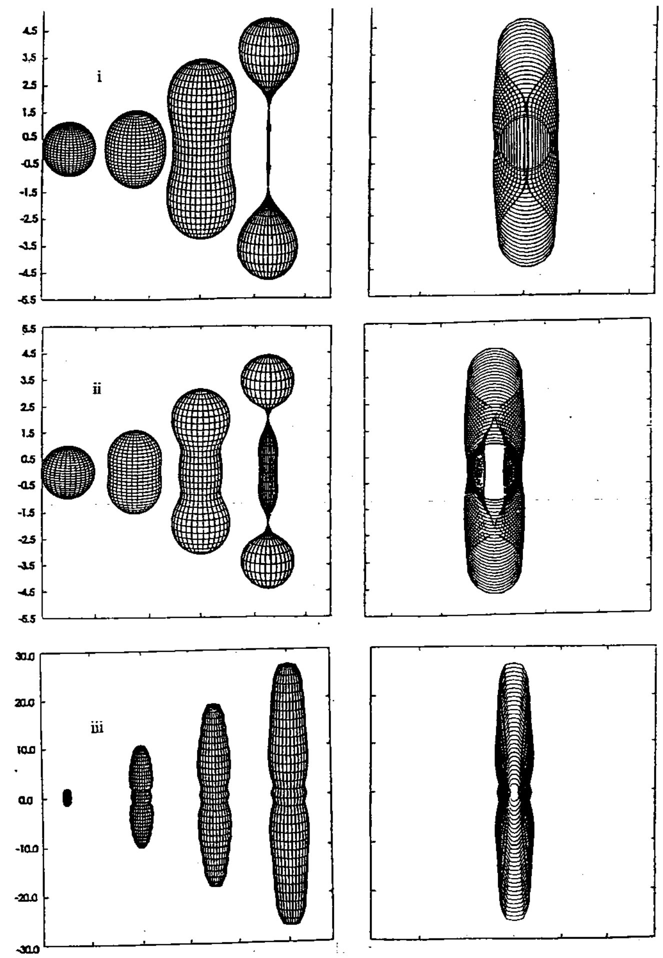

Figure 15: Bubble dynamics on the axis of a vortex line. Left side shows 3-D shapes at selected times, right side shows bubble contours at increasing times. a) Initial elongation ratio of 3, p_i/p_∞ i) No swirl, ii) $O = 0.56$, $R_c/R_{max} = 3$. b) $\Gamma = 0.005$ m^2/s, $R_o = 100$ μm. i) $p_i/p_\infty = 2$, $R_c/R_o = 1$, ii) $p_i/p_\infty = 1$, $R_c/R_o = 1$, iii) $p_i/p_\infty = 2$, $R_c/R_o = 0.57$. Reprinted from (25).

near a solid wall causes material erosion have been the subject of controversy for a long time. Indeed, a shock wave can be generated at bubble collapse (Fig. 2). In addition, bubble collapse near a solid surface proceeds with the formation of a damaging microjet. During its implosion the bubble first elongates perpendicular to the wall, then the side away from it flattens and a re-entering region is formed initiating a microjet which can pierce the bubble and hit the wall. Figure 5 shows a numerical simulation of this collapse using 2DynaFS. Very beautiful pictures of the phenomenon were taken by Lauterborn (20) who generated the bubbles using a laser. Figure 6 presents some of our high speed photographs using the spark generated bubbles (21).

Influence of fluid properties on the bubble behavior

Drag-reducing polymers are known to greatly reduce the cavitation inception index for several types of flows. The onset of cavitation is also delayed in acoustic cavitation in a stagnant fluid (16). In addition, cavitation erosion has been reported to be greatly modified (in both directions) with additives. Experimental (1) and theoretical (2,21) studies on a spherical bubble growth and collapse have shown no significant differences between a Newtonian and a viscoelastic fluid. This conclusion was supported by our high-speed photographic observations of spark-generated bubbles in an unbounded fluid (4).

However, these observations showed that a Polyox WSR 301 solution has a noticeable influence on non-spherical bubble dynamics near solid walls, compared to a liquid having the same viscosity (water + glycerin). The effect of the presence of the additives is to bring the bubble behavior closer to that of a spherical cavity. In order to compare bubble behavior in water and in a viscoelastic liquid, diluted polymer solutions of Polyox were used in the set up described above. In the first series of tests (11), a cylindrical aluminium specimen, used to record the damage due to the implosion, was fitted under the electrodes in a hole drilled in a Plexiglas plate. It was observed later, while analyzing the motion pictures, that this specimen, not being tight enough in the hole, was being slightly sucked up towards the bubble during its growth and then returned after the implosion.

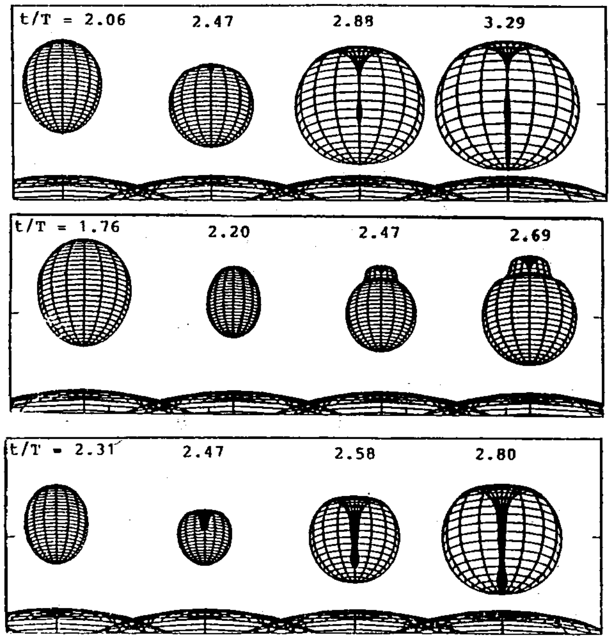

Figure 16: Comparison of calculated bubble collapse contours using 2DynaFS and Nike2D. Top to bottom: fixed, rigidly moving, and deforming structure. Reprinted from (26).

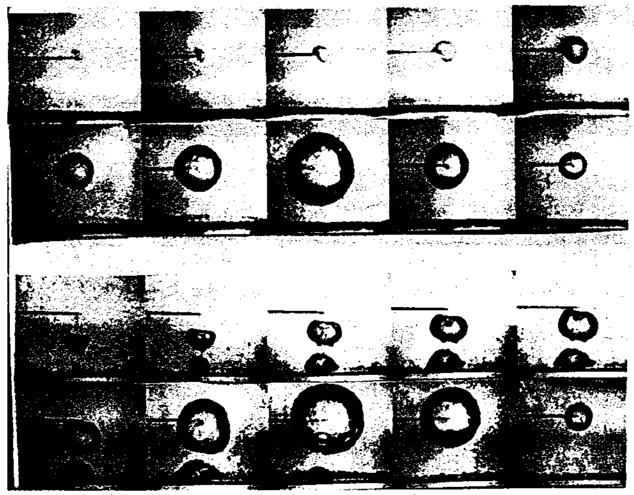

Figure 17: Collapse of spark-generated bubbles below a plate. a) Rigid 0.475 in. Plexiglas plate. b) Flexible 0.125 in. nylon plate.

This was in fact fortunate since it allowed the study of the influence of wall motion on the bubble dynamics. In that case the curves $R_A/R_{Cmax} = f(t/\tau_{sph})$(see Figure 7 also for definitions), where τ_{sph} is the period of oscillation of the spherical bubble obtained in the same conditions show that the period of oscillation of the bubble decreases when $\varepsilon = R_{Cmax}/l_o$ increases. This behavior, comparable to that near a free surface, is the opposite of what happens near a fixed solid wall.

The experiment was then repeated with a fixed wall. The lengthening effect on the bubble life was verified and increased with ε (Fig. 7). In both cases described above, the bubble was violently attracted towards the wall during its successive collapses and rebounds.

In the presence of polymer additives the following observations were made. In the vicinity of the moving solid wall, for the same ε, the addition of a 250 ppm of Polyox delayed the creation of the microjet thus increasing the bubble lifetime and moving the curves $R_A = f(t)$ toward the spherical case curve. Near a fixed solid wall the apparently opposite effect (shortening of the period of oscillation) in the presence of polymers was also seen to reduce the differences between the considered case (given ε) and the spherical case (11,12). This seems to indicate a stabilizing effect on bubble departure from sphericity due to the presence of the viscoelastic fluid. However, as shown in Figure 10, the opposite effect was observed in the presence of a free surface (12).

Behavior between two solid walls

The collapse of bubbles between two solid walls is interesting from the practical view point of cavitation in confined areas. The large deformations involved are also of interest from the fundamental dynamics point of view. When $\varepsilon < 1$, a bubble at equal distance from the walls first elongates parallel to the walls (direction of most freedom) during its growth, then perpendicularly when the implosion starts. Later the bubble constricts in the medium plane of symmetry and splits in two parts. This is observed experimentally in Figure 8 and simulated numerically in Figure 9 using the code 3DynaFS. Later on each of the two bubbles formed collapses with the formation of a microjet directed to the closer wall. When $\varepsilon \geq 1$, the bubble behaves as a cylindrical cavity until the final stages of collapse where it constricts and splits in two parts (7,9).

Quantitatively the presence of the two walls augments the bubble lifetime significantly. This lengthening effect increases dramatically with ε (Figure 10). When ε is approximately equal to 0.7 the period increases by 50% (compared to only 7% in the presence of a single wall) and when ε is approximately equal to 2 it is doubled.

In the presence of polymer additives a shortening of the period of oscillation tends, as for the single wall, to reduce the differences between the considered case and the spherical case.

Bubble collapse near a flat wall in a shear flow

While most numerical simulations and experimental observations of fundamental bubble dynamics have been made in a quiescent liquid near an infinite wall, it is obvious that cavitating bubbles most often occur in a

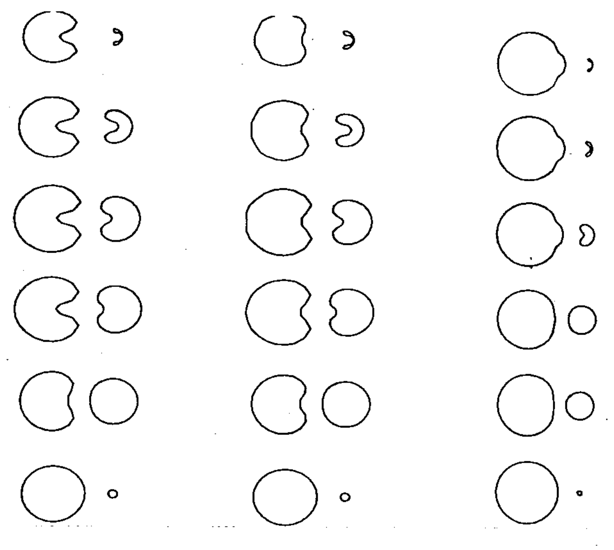

Figure 18: Simulation of the growth and collapse of a bubble near a globule. Bubble and globule shapes versus time. Indices 1 and 2 are for bubble and globule respectively. a) $R_{max1} = R_{max2}$, $\sigma_1 = \sigma_2 = 0.77$ *N/m*, $k_1 = 1.25$, $k_2 = 10$. b) $R_{max1} = R_{max2}$, $\sigma_1 = 0.77$ N/m, $\sigma_2 = 10^4$ *N/m*, $k_1 = 1.25$, $k_2 = 10$. c) $R_{max1} = 2R_{max2}$, $\sigma_1 = \sigma_2 = 0.77$ N^2/s, $k_1 = 1.25$, $k_2 = 10$.

flow with a slip velocity between the bubble and the liquid. These effects can be simulated numerically using 3DynaFS. Figure 11 illustrates the results of bubble behavior near a flat plate in the presence of a shear flow. The shear flow is such that $V_o = 0$ at the wall and grows linearly away from it to attain V_{shear} at the location of the bubble center. The figure shows interesting results for bubble behavior during bubble growth and collapse.

For an increasing ratio, $\tau = V_{shear}/\sqrt{\Delta_{P/\rho}}$, between the shear flow velocity and the characteristic bubble collapse velocity, the bubble deforms and elongates more and more during its growth. For small values of τ, the re-entering jet is deviated from the perpendicular to the plate with increasing values of τ. For larger values of τ, the re-entering jet formation is totally modified and the bubble tends to cut itself into a toroidal bubble. With increasing values of τ, an interesting lifting effect is observed, and the bubble centroid is seen to move further and further away from the wall. This results from an interaction between the shear flow and the rotation imparted to the bubble.

Interaction between multiple bubbles

In a cavitating flow field bubbles are seldom isolated, so there is a need for simulation tools for multibubble interactions. The first model we developed was based on matched asymptotic expansions (22). This model explained the fact that collective bubble dynamics can generate pressures much higher than expected from the simple addition of single bubble effects. This explains the very high erosion rates observed when cloud cavitation occurs. However, this model diverged when the number of bubbles increased or when the bubble spacing decreased. Using the BEM method, these limitations can be removed and more realistic and accurate results obtained. Figure 12 compares the results obtained with 3DynaFS with those using an asymptotic approach (22,24). Note that the asymptotic approach is already an improvement over most previous studies, which totally neglected the interactions. The bubble cloud is subjected to a sudden pressure drop, and cloud configurations of 1, 2, 4 and 8 bubbles are considered.

For the 2-bubble case the bubble centers are separated by a distance l_0, and the initial gas pressure in each bubble is such that the bubble would achieve a maximum radius $R_{max} = R_{b0} = 0.047l_0$ if isolated. The four-bubble configuration considers similar bubbles centered on the corners of a square with sides of dimension l_0. Finally, the eight bubbles are located on the corners of a cube of side l_0. The figure presents the variations with time of the pressure measured at the "cloud center" normalized by that obtained with an isolated bubble. As expected, the asymptotic approach gives a very good approximation for a small number of bubbles, *N*. However, the pressures predicted by the asymptotic analysis are seen to become much higher than the more accurate 3D results for an increasing value of *N*. Similar results are observed when the cloud void fraction or the ratio, $\varepsilon\pi = r_{bo}/l_o$, increases (24). This result qualifies earlier conclusions about extremely large pressures generated by a bubble cloud collapse.

Figure 13 illustrates another important effect due to asymmetries in a bubble cloud configuration. It considers an asymmetric five bubble configuration. All bubbles have the same initial radius and internal pressure, and are initially spherical and located in the same plane. The most visible effect is that observed on the center bubble; its growth is initially similar to that of the other bubbles, but it ends up being the least deformed. Later on, as the collapse proceeds with the development of a re-entrant jet directed towards the central bubble, this bubble appears to be shielded by the rest of the cloud. Its period is at least double that of the other bubbles. Very similar effects are seen when the number of bubbles is increased. Figure 14 shows a 21-bubble configuration, where again growth occurs without too much interference between the bubbles. However, collapse proceeds from the outer bubble shells towards the inside, indicating a cloud period of oscillation much larger than that of individual bubbles, as predicted by cloud cavitation models (8).

Bubble dynamics on the axis of a vortex

Let us now consider the case where the bubble is placed at the axis of a vortex line at $t = 0$ and starts to grow due to the excess between the internal pressure and the local ambient pressure. During the growth phase the bubble elongates along the vortex axis, then starts its collapse from a significantly elongated shape (25). As shown in Figure 15a, this elongation is not the key parameter to the subsequent bubble behavior. If the rotation velocity is neglected, the collapse would proceed as for elongated bubbles with two opposing jets formed at the bubble points along the axis (Fig. 14). However, the opposite effect with a radial jet forming is in general obtained when the rotation in the vortex flow is included. The bottom of Figure 14a illustrates this for particular values of the vortex circulation, Γ, and the normalized viscous core radius, $R_c = R_c/R_{max}$.

In Figure 15b, the initial pressures inside the bubbles are taken to be larger than the pressure on the vortex axis, and the bubbles are left free to adapt to this pressure difference. For a given value of the circulation (normalized parameter, [equ 30]), the bubble behavior strongly depends on the ratio of the core radius R_c to R_{max}. In all cases where R_{max} is larger than R_c, it appears that the bubble tends to adapt to the vortex tube of radius R_c. This could lead to various bubble shapes, as shown in Figure 15b, ending up with a very elongated bubble with a wavy surface for large values of R_{max}/R_c. The figure shows bubble contours at various times during growth and collapse for various values of the core radius, R_c, and the ratio of the initial bubble and ambient pressures. Also shown are selected 3D shapes of the bubbles at various times which have the advantage of being much more descriptive.

It is apparent from these figures that during the initial phase of bubble growth, radial velocities are large enough to overcome centrifugal forces and the bubble first grows almost spherically. Later on, the bubble shape starts to depart from the spherical and adapts to the pressure field. The bubble then elongates along the axis of rotation. Once the bubble has exceeded its equilibrium volume, bubble surface portions away from the axis - high pressure areas - start to collapse, or to return rapidly towards the vortex axis.

On the other hand, points near the vortex axis do not experience rising pressures during their motion, and are not forced back towards their initial position, thus continuing to elongate along the axis. As a result, a constriction appears in the mid-section of the bubble. The bubble can then separate into two or more tear-shaped bubbles. It is conjectured that this splitting of the bubbles is a main contributor to cavitation inception noise which can be used as a means of detecting cavitation.

Bubble collapse near deformable bodies

This section illustrates the importance of accounting for the motion and deformation of a nearby body in the study of bubble dynamics. This has been illustrated indirectly in the above experiments, where the motion of an impacted sample significantly modified the history of the jet point. Figure 16 shows the behavior of a large bubble near a spherical structure. Three characteristic interaction cases are considered (26). In the first case the sphere is rigid and does not move or deform. In that case, as for a bubble collapsing near an infinite wall, the bubble collapse proceeds with the formation of a re-entering jet perpendicular to the sphere. In the second case, the sphere is allowed to move rigidly in response to the bubble pressure field. A very significant modification of the bubble behavior is observed, leading to a constriction of the bubble top prior to the formation of the re-entering jet. Finally, in the third case, a full coupling between the structure motion and deformation and the bubble behavior is considered using the coupled 2DynaFS and Nike2D codes. In that case, a bubble behavior between the above two cases is observed. A re-entering jet is still formed, but it is wider and slower than that achieved in the presence of a rigid sphere. However, the pressure felt by the deforming structure is larger (26).

Figures 17a and 17b compare the experimental observations of large spark-generated bubble behavior near a solid and a flexible plate. In both cases, a relatively large bubble is generated through a reduced ambient pressure in the bubble chamber, and the bubbles are spark-generated below horizontal plates. In Figure 17a, the plate is made of thick Plexiglas (0.475 inch), while in Figure 17b, the plate is made of thin (0.125 in) pliable plastic. The bubbles are generated under identical conditions and would have the same radius if in an infinite medium. The difference in the behavior of the two bubbles is, however, very obvious. Two important characteristics of the rigid wall case are the formation of a bubble re-entering jet directly towards the plate, and the reflection of an expansion wave at the plate wall which creates a secondary bubble from minute air bubbles trapped under the plate (Fig. 17a).

In the flexible wall case shown in Figure 17b, the re-entering jet is practically eliminated, and the bubble collapses almost spherically without moving towards the plate. Due to some asymmetry in the plate position relative to the bubble, a small motion sideways and away from the plate is observed. The formation and growth of a bubble layer near the solid plate is replaced in the flexible plate case with a very fine sheet of tiny bubbles which move away from the plate. This again illustrates the importance of nearby wall motion and deformation on bubble dynamics.

Bubble collapse near simulated cells

The last example presented in this communication concerns the behavior of a bubble near simulated blood cells. Undesirable effects of cavitation using ultrasound have been reported in the literature (8). The negative effects of cavitating bubbles on nearby cells are explained by the impact of re-entering jets on the cells and by the generation of large stresses on the cell. Without trying to simulate accurately the cell globule, we have considered the interaction of a growing and collapsing bubble and a nearby spherical globule with a very high surface tension and/or a very low compressibility content. The bubble behavior near such a simulated cell is seen to depend on the size ratio between the bubble and the globule.

In most cases, as in Figures 18a and b, the cell acts as a nearby free surface and tends to repel the re-entering jet formed during the bubble collapse. This jet moves away from the globule. However, it appears that the globule is seen subjected to very high stresses leading to a sharp intrusion of the fluid in the globule and a potential rupture of the globule interface. Figure 18c shows a second configuration where the globule is much larger than the bubble, in which case the globule is stretched in a different fashion.

Conclusions

We have reviewed various aspects of cavitation inception and highlighted the potential for error in scaling if the proper definition is not used. For instance, the concept of nuclei distribution in the cavitating medium, often not addressed, can be a source of serious scaling problems. A few models for bubble growth and collapse were then presented, including the effects of a non-Newtonian fluid which are of relevance to biological applications. The importance of non-spherical bubble dynamics was then addressed as this is very common in any conditions where cavitation erosion occurs. The influence of relative liquid bubble flow, multibubble interactions and the presence of non-uniform flow fields were then briefly considered. Finally, the importance of the inclusion of the motion and deformation of the nearby boundaries or cells was highlighted.

While this communication addressed a host of problems, showing some particular solutions, it was not able to give definite general conclusions. It did, however, highlight the fact that the study of cavitation is much more complex than usually thought. Simplified, commonly used models (spherical and axisymmetric) can lead to simplified answers. However, these results are only good in very limited conditions, and risk results that can be in error by orders of magnitudes. Fortunately, with recent advances in computational techniques and computers, detailed simulations of particular conditions are becoming more and more within reach.

Acknowledgements

Major parts of this paper are based on work supported by the Office of Naval Research, Contract N00014-89-C-0025. The author would like to acknowledge the contributions of several colleagues at Dynaflow, particularly Drs. Ramani Duraiswami and Kenneth Kalumuck.

References

1. Besant WH. Hydrostatics and hydrodynamics. Cambridge University Press, London, 1859:Art. 158
2. Lord Rayleigh. On the pressure developed in a liquid during collapse of a spherical cavity. Phil Mag 1917;34:94-98
3. Brown B, Goodman JE. High intensity ultrasonics - industrial applications. Ilife Books ltd., London, 1965
4. Chahine GL, Johnson VE Jr. Mechanics and applications of self-resonating cavitating jets. ASME International Symposium on Jets and Cavities, WAM, Miami, Florida, 1985;FED-Vol.31:21-35
5. Chahine GL, Johnson VE Jr, Lindenmuth WT, Frederick GS. The use of self-resonating cavitating water jets for underwater sound generation. J Acoustical Soc Am 1985;77-1:113-126
6. Knapp RT, Daily JW, Hammitt FG. Cavitation. McGraw Hill Book Co., NY, 1970
7. Hammitt FG. Cavitation and multiphase flow phenomena. McGraw-Hill International Book Co., NY, 1980
8. Young FR. Cavitation. McGraw Hill Book Co., NY, 1989
9. Plesset MS, Prosperetti A. Bubble dynamics and cavitation. Ann Rev Fluid Mech 1977;9:145-185
10. Chahine GL. Etude asymptotique et experimentale des oscillations et du collapse des bulles de cavitation. Docteur Ingenieur Thesis, Universite Paris VI, Pierre et Marie Curie, 1974
11. Chahine GL, Fruman DH. Dilute polymer solution effects on bubble growth and collapse. Physics of Fluids 1979;22(7):1406-1407
12. Chahine GL. Experimental and asymptotic study of non-spherical bubble collapse. Appl Scientific Res 1982;38:187-197
13. Alloncle AP, Dufresne D. Visualization of laser induced vapor bubbles and pressure waves. Proceedings, IUTAM Symposium on Bubble Dynamics and Interface Phenomena, Birmingham, 6-9 Sept. 1993;(in press)
14. Rood EP. Cavitation Inception Research - Focus and Direction. Report on the "Advisory Council on Cavitation Events" ONR meeting on May 20th 1992 in Memphis TN.
15. Gilmore FR. The growth and collapse of a spherical bubble in a viscous compressible liquid. California

Institute of Technology Report 26-4, California, 1952
16. Cole RH. Underwater explosions. Dover Publications, 1948
17. Chahine GL, Perdue TO, Tucker CB. Interaction between an underwater explosion and a solid submerged body. Dynaflow, Inc. Technical Report, 89001-1, Sep. 1988
18. Chahine GL. Nonspherical bubble dynamics in a line vortex. Proceedings of ASME 1990 Cavitation and Multiphase Flow Forum, Toronto, Canada, 1990;FED-Vol.98:121-127
19. Chahine GL. Numerical modelling of the dynamic behavior of bubbles in nonuniform flow fields. ASME symposium on numerical methods for multiphase flows, Toronto, Canada, 1990;FED-Vol.91:57-65
20. Lauterborn W. Cavitation and coherent optics. In: Lauterborn W (ed). Cavitation and inhomogeneities in underwater acoustics. Springer Verlag, 1980:3-13
21. Chahine GL. Etude locale du phenomene de cavitation. Analyse des facteurs regissant la dynamique des interfaces. Docteur d'Etates-Sciences Thesis, Université Pierre et Marie Curie, April, 1979
22. Chahine GL. Cloud cavitation: theory. 14th Symposium on Naval Hydrodynamics, Ann Arbor, Michigan, National Academy Press, Washington, DC, 1983:165-195
23. Chahine GL. Dynamics of the interaction of nonspherical cavities. In: Miloh T (ed). Mathematical approaches in hydrodynamics. SIAM, Philadelphia, 1991:51-68
24. Chahine GL, Duraiswami R. Dynamical interactions in a multi-bubble cloud. ASME, J Fluids Eng 1992;114:680-687
25. Chahine GL. Bubble interaction with vortices. In: Green S (ed). Fluid vortices Kluwer Academic Publishers 1994:(in press)
26. Chahine GL, Kalumuck KM, Duraiswami R. Coupling of a fluid's BEM code with a structural FEM code for fluid-structure interaction simulation. Boundary Element XV, Vol.1. Stress Analysis. Brebbia CA Rencis JJ (eds). CMP, Elsevier, 1993:581-597

Discussion

Swanson:
This photography is to be commended. One of the things that I would like to point out specifically is that in the very last series there were a number of rebounds for those bubbles. As the bubbles collapse, the generated jet does all those damages. These are the prettiest pictures I have seen in a long time.

Chahine:
Thank you.

Israelachvili:
How do you know that the damage is not caused by the spark? I would like to show some pictures given to me by Professor Ellis before he died. These pictures show that the shock waves at the inception are as strong as they are when they collapse.

Chahine:
The subject of what generates the erosion, the shock or the re-entering jet, is very old as we saw from Professor Ellis' picture. I think that it is a combination of both effects and depending upon the bubble distance from the wall and what configuration is used it is one rather than the other. For example, in an underwater explosion it would be much more the shock. However, we have been working on instances where it is the jet that is much more erosive than the shock.

Regnault:
Maybe you can clear up a few concerns or questions I have about cavitation. You defined cavitation as the expansion of nuclei bubbles and the recollapse of those as opposed to the generation of vapor without a nuclei. Is that correct?

Chahine:
I have no doubt in my mind that it is practically impossible to generate vapor out of no nuclei. I think maybe 95% of the cavitation community would agree.

Regnault:
In the case of cavitation in the body where we would have a large amount of dissolved gases, would you say that the drawing out of dissolved gases from the bloodstream then the recollapse of these bubbles would be the source for cavitation bubbles?

Chahine:
No, I think there is a confusion between dissolved gases and gases that are in suspension as nuclei. In the first set, the molecules of the gas are mixed with the molecules of the water. The characteristic time for these dissolved gases to go into the nuclei is very long. That is not what I am talking about. I am talking about actual microscopic bubbles that are already present in the liquid, very different from the dissolved gases in the bloodstream.